HEXIM1 is correlated with Alzheimer's disease pathology and regulates immediate early gene dynamics in neurons

Myo Htet[1], Camila Estay-Olmos[1], Lan Hu[2], Yiyang Wu[3], Brian E. Powers[1], Clorissa D. Campbell[4], M. Rafiuddin Ahmed[4], Timothy J. Hohman[3,5], Julie A. Schneider[6], David A. Bennett[6], Vilas Menon[7], Philip L. De Jager[7], Garrett A. Kaas[8], Roger J. Colbran[2], Celeste B. Greer[1*]

[1]Mol. Pharmacol. and Neurosci., Loyola Univ. Chicago Hlth. Sci., Maywood, IL, 60153, USA
[2]Dept. Molec. Physiol. & Biophysics, Vanderbilt Univ., Nashville, TN, USA
[3]Vanderbilt Memory and Alzheimer's Ctr., Vanderbilt Univ. Med. Ctr., Nashville, TN, USA
[4]Dept. Pharmacol., Vanderbilt Univ., Nashville, TN, USA
[5]Ctr. for Human Genet., Vanderbilt Univ. Med. Ctr., Nashville, TN, USA
[6]Rush Alzheimer's Disease Ctr., Rush Univ. Med. Ctr., Chicago, IL, USA
[7]Center for Translational & Computational Neuroimmunology, Dept. of Neurology, and the Taub Institute for Research on Alzheimer's disease and the Aging Brain, Columbia Univ. Irving Med. Ctr., New York, NY, USA
[8]Genet. Med., Vanderbilt Univ. Med. Ctr., Nashville, TN, USA
*Corresponding author: cgreer@luc.edu

ABSTRACT

Impaired memory formation and recall is a distinguishing feature of Alzheimer's disease, and memory requires de novo gene transcription in neurons. Rapid and robust transcription of many genes is facilitated by the formation of a poised basal state, in which RNA polymerase II (RNAP2) has initiated transcription, but is paused just downstream of the gene promoter. Neuronal depolarization releases the paused RNAP2 to complete the synthesis of messenger RNA (mRNA) transcripts. Paused RNAP2 release is controlled by positive transcription elongation factor b (P-TEFb), which is sequestered into a larger inactive complex containing Hexamethylene bisacetamide inducible protein 1 (HEXIM1) under basal conditions. In this work, we find that neuronal expression of *HEXIM1* mRNA is highly correlated with human Alzheimer's disease pathologies. Furthermore, P-TEFb regulation by HEXIM1 has a significant impact on the rapid induction of neuronal gene transcription, particularly in response to repeated depolarization. These data indicate that HEXIM1/P-TEFb has an important role in inducible gene transcription in neurons, and for setting and resetting the poised state that allows for the robust activation of genes necessary for synaptic plasticity.

GRAPHICAL ABSTRACT

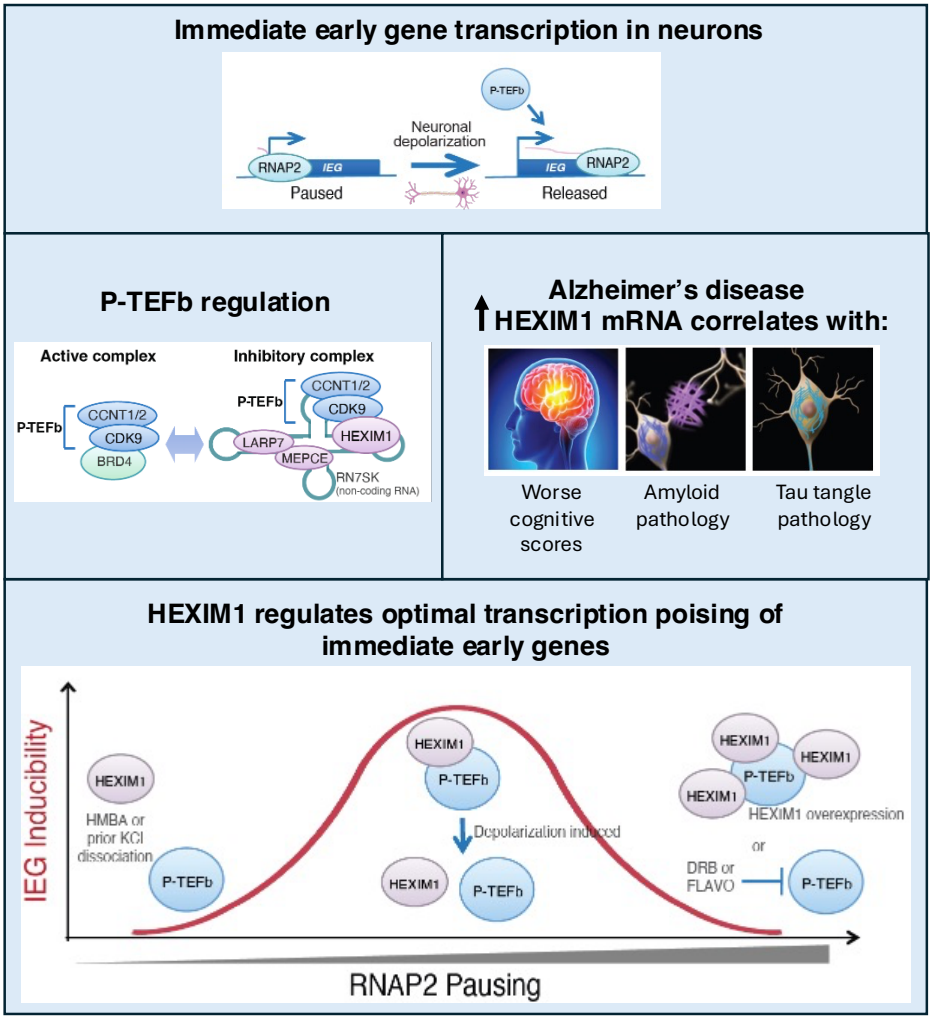

INTRODUCTION

Alzheimer's disease (AD) is an aging-associated neurodegenerative disorder that leads to progressive cognitive impairment and memory loss. The accumulation of neurofibrillary tangles comprised of Tau and amyloid beta (Aβ) plaques in the brain are well-established biomarkers of this destructive disease. There is a growing appreciation that AD is also associated with alterations in gene expression in a variety of cell types in the brain, and transcription is especially perturbed in neurons (Mathys *et al*, 2019).

Learning and memory formation require carefully orchestrated changes in gene transcription programs by RNA polymerase II (RNAP2) that are induced by increased synaptic activity (Alberini & Kandel, 2014; Medina *et al*, 2019; Thut & Lindell, 1974). Immediate early genes (IEGs) are rapidly and transiently induced in response to neuronal activation. IEGs encode proteins that promote neuronal plasticity (Activity regulated cytoskeleton associated protein, *Arc*; *Homer1*; etc.) and several transcriptional activators (*Fos*; Early growth response factor 1, *Egr1*; *Jun*; Neuronal PAS domain protein 4, *Npas4*; Nuclear receptor subfamily 4 group A member 2, *Nr4a2*; etc.). IEGs are induced in the hippocampus by a variety of cognitive processes (Clayton, 2000; Guzowski *et al*, 2001; Kaczmarek, 2000; Strekalova *et al*, 2003; Teather *et al*, 2005). Recent work has identified that repeated stimulations of neurons lead to damped successive transcriptional responses of IEGs (Rienecker *et al*, 2022). However, molecular mechanisms underlying the dampened response to serial stimuli remain unknown. Moreover, the potential recovery from transcriptional dampening and the role of transcriptional dampening in human disease has not been investigated.

Activation of IEGs in neurons occurs via the process of RNAP2 pause and release (Saha *et al*, 2011). Studies in other cell types have shown that RNAP2-dependent synthesis of new messenger RNAs occurs in phases as the polymerase transitions between initiation, pausing, elongation, and termination. Positive transcription elongation factor b (P-TEFb) releases RNAP2 into the elongation phase (Marshall & Price, 1995). P-TEFb is a heterodimer of cyclin-dependent kinase 9 (CDK9) and either Cyclin T1 or T2 (CCNT1 or CCNT2). When actively inducing elongation, P-TEFb associates with bromodomain-containing protein 4 (BRD4) (Jang *et al*, 2005), an acetyl-lysine binding protein that targets active P-TEFb to acetylated histones surrounding active gene promoters that contain paused RNAP2. Alternatively, association of the P-TEFb heterodimer with Hexamethylene bisacetamide inducible protein 1 (HEXIM1) restricts P-TEFb activity (Yik *et al*, 2003). This transcriptional silencing complex also contains methylphosphate capping enzyme (MEPCE), La-related protein 7 (LARP7), and the non-coding RNA RN7SK (Krueger *et al*, 2008). Despite the importance of this complex in other cell types, the specific role of the P-TEFb inhibitory complex is only recently beginning to be investigated in the brain (Park *et al*, 2023).

Several reports show IEGs are misregulated in aging and AD (Canchi *et al*, 2019; Choi *et al*, 2019; Desjardins *et al*, 1997; Espana *et al*, 2010; Marcus *et al*, 1998; Myrum *et al*, 2022), and that altering transcription pause release pharmacologically in rodent models rescues IEG expression (Chen *et al*, 2021; Faraji *et al*, 2023). Therefore, factors regulating pausing could be effective AD targets, and there are several examples of pause release inhibitors improving cognitive functions in AD model organisms. First, flavopiridol, a P-TEFb inhibitor, improved passive avoidance and object recognition memory in Aβ oligomer-injected mice (Leggio *et al*, 2016). BRD4 inhibition has been shown to improve memory in some (Badrikoohi *et al*, 2022; Benito *et al*, 2017; Faraji *et al.*, 2023; Nikkar *et al*, 2022), but not all (Magistri *et al*, 2016) rodent models of Aβ accumulation. Inhibitors of histone deacetylases (HDACs) also decrease transcription

pause release (Greer *et al*, 2015; Kim *et al*, 2013; Marie *et al*, 2018; Sanchez *et al*, 2018), and improve memory in mice with Aβ accumulation (Athaide Rocha *et al*, 2023; Francis *et al*, 2009; Kilgore *et al*, 2010; Su *et al*, 2021; Wang *et al*, 2014). These works highlight that understanding transcription pausing in neurons might lead to insights that could help treat the cognitive symptoms of AD.

We set out to determine whether, P-TEFb, is altered in AD. Using postmortem human data (De Jager *et al*, 2018), we find that expression levels of certain subunits of P-TEFb and components of the P-TEFb inhibitory complex are correlated with AD pathology across several brain regions. In particular, *HEXIM1* is highly dysregulated, and single nuclei RNA sequencing (snRNA-seq) reveals correlations between its expression and declining cognition and neurofibrillary tangles in neurons. Therefore, we investigated the function of HEXIM1 and its effect on P-TEFb regulation of IEG induction using primary mouse hippocampal neuron cultures. Using pharmacological and genetic approaches, we identify that HEXIM1 sequestration of P-TEFb primes neurons to activate IEGs in response to depolarization. After IEG activation, there is a period where neurons cannot reactivate certain IEGs as robustly, but they eventually recover after several hours. This timeline coincides with a period of decreased HEXIM1 protein expression, and the dampened response to stimuli during this period is P-TEFb-dependent. As a whole, our work identifies that neuronal *HEXIM1* expression is dysregulated in AD and implicates HEXIM1 as an important modulator of the gene expression changes that follow neuronal depolarizations.

RESULTS

Due to the possible link between AD and regulators of transcriptional pausing, we sought to understand how cognition and AD-associated pathologies correlated with the expression of mRNAs related to pause release. A strength of the Religious Orders Study/Memory and Aging Project (ROSMAP) study is that subjects enrolled well before pathology developed and provided antemortem cognitive assessments over a period of time. Postmortem, their brain tissue was analyzed for pathological markers (Bennett *et al*, 2005) and subjected to transcriptional analysis (De Jager *et al.*, 2018). We used this dataset to examine the correlation between mRNA expression of several P-TEFb regulators (*BRD4*, *CCNT1*, *CCNT2*, *CDK9*, *HEXIM1*, *LARP7*, *MEPCE*, and *RN7SK*) and AD-associated phenotypes. Correlations with cognitive scores in study participants from their final clinical evaluation prior to death (Cross-sectional cognition; **Fig. 1A**), change in cognitive assessment scores across time (Longitudinal cognition; **Fig. 1B**), amyloid pathology (**Fig. 1C**) and tau tangle pathology (**Fig. 1D**) were assessed in the head of the caudate nucleus (CN). We saw significant correlations between several of these genes and AD-pathologies (FDR < 0.05), with *HEXIM1* being among the most significantly altered genes across all categories examined. It correlated with poorer cognitive scores and increased amyloid and Tau pathologies. Other components of the inhibitory complex (*MEPCE* and *LARP7*) and a component of P-TEFb (*CDK9*) were also significantly correlated in the same direction as *HEXIM1* (**Fig. 1A-D**). *HEXIM1, MEPCE* and *LARP7*, unlike *CDK9*, were similarly correlated with AD pathology in other brain areas (dorsolateral prefrontal cortex (DL-PFC), and posterior cingulate cortex (PCC) (**Supp Fig. 1A-H**).

Because these correlations were identified from bulk tissue, we next sought to determine if P-TEFb inhibitory complex component associations with AD could be attributed to a particular cell type. To this end, we analyzed expression levels of these genes in publicly available single nucleotide RNA sequencing (snRNA-seq) data set generated from ROSMAP samples. Neurons were clustered into three types (excitatory cut-like homeobox 2 (cux2) positive (ex

cux2+), excitatory cux2 negative (ex cux2-), and inhibitory (inhib)). Cux2 is expressed in layers II-IV of the cortex (Cubelos *et al*, 2010; Yang *et al*, 2020). Additionally, five non-neuronal cell types (astrocytes (ast), endothelial cells (endo), microglia (micro), oligodendrocytes (oligo), and oligodendrocyte progenitor cells (opc)) were defined. Amongst the components of the inhibitory complex, *HEXIM1* had several correlations with AD pathology in neuronal subtypes (**Fig. 1E**). Longitudinal cognition was negatively correlated with *HEXIM1* expression in ex cux2- neurons, and tangles were positively correlated with *HEXIM1* expression in all neuronal subtypes (**Fig. 1E**). *MEPCE* (**Fig. 1F**) and *LARP7* (**Fig. 1G**) also correlated with AD pathology, but in non-neuronal cell types. *MEPCE* expression is positively correlated with amyloid in micro cells. *LARP7* was negatively correlated with longitudinal cognition in ast cells, but positively correlated in endo cells. *LARP7* expression is also positively correlated with amyloid in ast, olig, and opc cells. These data suggest that while AD is associated with *LARP7* and *MEPCE* expression in a variety of non-neuronal cell types, the *HEXIM1* expression correlations were found in neurons. However, very little is known about *HEXIM1* function in neurons.

Given these findings, we next asked if HEXIM1 might play a role in neuroplasticity. Therefore, we examined a publicly available RNA-seq dataset (Kennedy *et al*, 2016) generated from animals during memory formation. We observed a significant increase in *Hexim1* mRNA expression in mouse CA1 hippocampus region 1 hour following a mild memory-inducing foot shock (**Fig. 2A**). To directly determine whether HEXIM1 protein is expressed in neurons, we cultured primary hippocampal neurons from mice. HEXIM1 protein is co-expressed with the TUJ1 neuronal marker and has a nuclear localization (**Fig. 2B**). To test if *Hexim1* mRNA expression is activity-dependent, as suggested by the fear conditioning experiment, we depolarized these cells with potassium chloride (KCl) (Rienecker *et al*, 2020), and saw a significant increase in *Hexim1* mRNA (**Fig. 2C**). To examine this transcriptional change in another cell system, we used Neuro2a cells that were differentiated (differentiated N2a; or dN2a), and likewise saw an increase *Hexim1* mRNA in response to KCl (**Supp. Fig. 2**). Taken together, these data suggests that neurons express HEXIM1 protein, and dynamically regulate *Hexim1* mRNA expression in response to memory formation and neuronal depolarization.

We next sought to test if HEXIM1 might also influence IEG induction in neurons. Therefore, we generated an adeno-associated virus of serotype 9 (AAV9) to overexpress Flag-tagged recombinant mouse *Hexim1* under the control of the neuron-specific promoter human synapsin 1 (hSyn1). The recombinant protein runs at a slightly higher molecular weight due to the Flag tag (**Fig. 3A**). Both control virus and hSyn1:F:*Hexim1* expression viruses also express enhanced yellow fluorescence protein (eYFP) from a constitutive eukaryotic promoter, and viral transduction led to similar levels of eYPF expression **(Fig. 3B)**. HEXIM1 overexpression dampened KCl-dependent IEG induction for *Fos* (**Fig. 3C**), *Arc* (**Fig. 3D**), and *Egr1* (**Fig. 3E**). *Nr4a2* showed a non-significant trend towards suppressed activation of its expression (**Fig. 3F**). These findings show that too much HEXIM1 blunts IEG induction, and HEXIM1 plays a direct role in modulating IEG inducibility.

HEXIM1 in other cell types binds P-TEFb to suppress its activity (Barrandon *et al*, 2007; Fujinaga *et al*, 2012; Yik *et al.*, 2003). Therefore, we tested whether these two interact in the hippocampus, and whether P-TEFb is involved in IEG induction by KCl in primary neurons. We found that CDK9, the kinase subunit of P-TEFb, coimmunoprecipitates with HEXIM1 from hippocampal protein lysates and vice versa, suggesting they are associated in the hippocampus (**Fig. 4A**). The higher molecular weight CDK9-55 kDa isoform (Shore *et al*, 2005) seems to show preferential association with HEXIM1. We next asked whether small molecule inhibitors of P-

TEFb influenced immediate early gene activation in neurons. Inhibiting P-TEFb with 5,6-Dichloro-1-β-D-ribofuranosylbenzimidazole (DRB) leads to suppressed activation of *Fos* (**Fig. 4B**), *Arc* (**Fig. 4C**), *Egr1* (**Fig. 4D**), and *Nr4a2* (**Fig. 4E**) relative to cells treated with DMSO vehicle control. We further sought to test this effect on the same genes with a second structurally dissimilar P-TEFb inhibitor, Flavopiridol (FLAVO) that exhibits a higher potency than DRB (Baumli *et al*, 2010; Lu *et al*, 2015; Ni *et al*, 2020). This treatement revealed a similar significant suppression of IEG induction by KCl (**Fig. 4F-I**). The increased *Fos* and *Egr1* expression by KCl is also suppressed by the same two drugs in dN2a (**Supp. Fig. 4**). Together, we see that the P-TEFb complex that associates with HEXIM1 in the hippocampus modulates stimulus-dependent IEG induction in neurons, presumably by preventing RNAP2 pause release.

Next, we investigated whether the disruption of P-TEFb sequestration by HEXIM1 affects activity-dependent IEG expression. We therefore used the drug that is the namesake of HEXIM1, hexamethylene bisacetamide (HMBA), which transiently dissociates HEXIM1 from P-TEFb (Contreras *et al*, 2007), freeing P-TEFb to induce elongation unrestricted from the effects of the inhibitory complex (**Fig. 5A**). As reported in other cell types, HMBA treatment increased *Hexim1* mRNA expression in neurons (**Fig. 5B**) and dN2a (**Supp Fig. 5A**). However this short-term treatment with HMBA is insufficient to increase in HEXIM1 protein levels (**Supp Fig. 5B**). HMBA had somewhat different effects on the expression of *Fos* (**Fig. 5C**), *Arc* (**Fig. 5D**), *Egr1* (**Fig. 5E**), and *Nr4a2* (**Fig. 5F**) under basal conditions. Both *Fos* and *Egr1* were significantly induced by HMBA, *Arc* was trending towards an increase, but was not statistically significant, and *Nr4a2* was unchanged. However, HMBA pre-treatment attenuated the KCl-dependent induction of all these genes (**Fig. 5G-J**). A similar induction of baseline and suppression of induction was obtained in dN2a cells (**Supp Fig 5C-F**). These results suggest that HEXIM1 is necessary for poising inducible genes under basal conditions so that transcriptional pause release and mRNA expression can be rapidly induced by P-TEFb in response to neuronal stimulation.

Our initial examination of HEXIM1 function in neurons suggested that precluding HEXIM1 sequestration of P-TEFb or neuronal activation induces paused RNAP2 to clear out from IEG promoters. Therefore, following stimulation, RNAP2 will need to reengage with IEG promoters and advance to the pause site to restore the basal state. This requires the re-sequestration of P-TEFb by HEXIM1 in the inhibited complex. Therefore, we were interested to see how HEXIM1 is impacted during recovery from a KCl stimulation. We followed HEXIM1 protein levels for 4, 6, or 24 hours after KCl was removed from the cells (**Fig. 6A**). HEXIM1 protein is decreased 6 hr after KCl and recovered back to baseline levels 24 hrs later (**Fig. 6B**). We observed reciprocal changes in the levels of HEXIM1 mRNA along this same timeline in primary neurons (**Fig. 6C)** and in dN2a (**Supp Fig. 6**), suggesting cells synthesize more *Hexim1* mRNA to restore HEXIM1 protein levels by 24 hours. Therefore, we hypothesize that this may help the cell prepare for another bout of IEG induction.

We postulated that a delay in the gene reset process (reflected by the loss of HEXIM1 protein observed in **Fig. 6B**) might result in a refractory period in which transcriptional responses to a second round of neuronal activation, delivered prior to re-establishment of the basal/paused state, would be diminished. Indeed, other groups have observed dampened responses of IEGs in response to successive stimuli (Guzowski *et al*, 2006; Rienecker *et al.*, 2022). Therefore, we stimulated cells with KCl for 30 min., allowed them recover for 1 hr. after washing that out, then stimulated them with KCl for 30 min. again. At these shorter time scales, unprocessed pre-mRNA expression was assessed for rapid gene transcription activation. We found that KCl-

dependent transcriptional induction of *Fos*-, *Arc*-, *Egr1*-, and *Nr4a2*-pre-mRNA is significantly dampened when a prior KCl is administered (**Supp Fig. 7A-E**). However, we saw HEXIM1 protein repression at much longer timescales. This led us to speculate that recovery of transcriptional responses may take longer than 1 hr, so we used longer KCl treatments and a timecourse of recovery times. Consistent with our hypothesis, we see that *Fos* mRNA expression is not as strongly induced with a 2 hr. recovery period following a 2 hr KCl treatment as it is in cells naïve to a prior KCl. However, its induction is not significantly dampened after a 4 or 24 hr. recovery period (**Fig. 7B**). Similarly, *Egr1* shows the same pattern of dampened response and recovery (**Fig. 7D**). Like the primary neurons, dN2a show a diminished response in these same genes to a secondary stimulation 2 hrs. after a prior one (**Supp Fig. 7F-G**). Curiously, *Arc* inducibility is enhanced when stimulated again after 4 hrs of recovery (**Fig. 7C**), and *Nr4a2* appears to not have a reduced response (**Fig. 7E**), signifying there are gene-specific differences in secondary depolarization responses.

We next asked if the dampened response of *Fos* and *Egr1* to the second KCl stimulation is a direct consequence of P-TEFb activity, as we predict it is released from HEXIM1 and requires time for a reset of a baseline state. To address this question, we tested if inhibiting P-TEFb during the first KCl stimulation prevents suppression of KCl-dependent IEG induction we observed in the second stimulation. DRB or vehicle control (DMSO) was added to dN2a cells prior to the initial KCl stimulation. DRB was chosen as the P-TEFb inhibitor for this experiment rather than Flavopiridol because of its ability to be more efficiently washed away(Chao & Price, 2001). Both drug and KCl were washed out thoroughly, and cells recovered for 2 hrs before the second KCl stimulation in the absence of DRB (**Fig. 8A**). Following these treatments, we observed that the presence of DRB during the first stimulation significantly lessened the dampened response to KCl in the second stimulation for *Fos* (**Fig. 8B**) and *Egr1* (**Fig. 8C**), with *Fos* almost fully recovering to normal induction levels. Additional controls were conducted to test for potential residual effects of the DRB treatment after washout (**Supp. Fig. 8**). Cells were treated with DMSO or DRB, then only received the second KCl stimulation or water control. The prior DRB treatment had no effect on the expression of either IEG in the absence of KCl. However, while *Fos* fully recovered from having DRB applied previously, *Egr1* induction by KCl was still inhibited even after DRB washout. Therefore, the incomplete rescue of *Egr1* in **Fig. 8C** could be due to residual effects of DRB on *Egr1* transcription. Our results indicate that P-TEFb release of paused RNAP2 during the first stimulation may lead to the IEG not being poised for activation by a second stimulation.

DISCUSSION

Little is known about the role of P-TEFb regulators in AD, though they have been linked to other brain diseases and disorders (Alazami *et al*, 2012; Schneeberger *et al*, 2019; Singh & Sartor, 2020). *HEXIM1* was previously suggested to be dysregulated in AD (Pang *et al*, 2019), and we show here that *HEXIM1* expression is correlated with worse neuropathology and cognition, with particular associations arising between Tau pathology and longitudinal cognition in neurons. HEXIM1 was also increased in excitatory neurons in human AD across several brain regions in a separate snRNA-seq cohort (Mathys *et al*, 2024). Inhibitors that block pause release have deomonstrated therapeutic effects in AD model organisms (Athaide Rocha *et al.*, 2023; Badrikoohi *et al.*, 2022; Benito *et al.*, 2017; Faraji *et al.*, 2023; Francis *et al.*, 2009; Kilgore *et al.*, 2010; Leggio *et al.*, 2016; Nikkar *et al.*, 2022; Su *et al.*, 2021; Wang *et al.*, 2014). With this in mind, there are a few possible explanations for our seemingly paradoxical finding that

HEXIM1 mRNA is increased in human AD neurons, which would be predicted to also repress transcription pause release. First, blocking pause release via HEXIM1 upregulation could be a protective response of the brain to AD pathology, so furthering this block with pause release inhibitors would be beneficial to memory function. Second, it is important to point out that we do not yet know if the HEXIM1 protein is increased or decreased in AD. If it is decreased, *HEXIM1* mRNA could be increased in an effort to recover decreased protein levels, as we observed following our KCl stimulations (**Fig. 6**). Despite not yet fully understanding the role of HEXIM1 in AD, HEXIM1 dysregulation affecting IEG inducibility could create a possible mechanistic link explaining cognitive impairments in AD, as IEGs are crucial to memory formation (Fleischmann *et al*, 2003; Grimm *et al*, 1997; Guzowski *et al*, 2000; Savell *et al*, 2016; Zalcman *et al*, 2015). Thus, we felt it was important to investigate the role of HEXIM1 on IEGs in neurons.

We observed that *Hexim1* mRNA is increased in the hippocampus during memory formation. Other groups have identified that the levels of hippocampal *Hexim1* mRNA are significantly increased in mRNA expression datasets. For example, *Hexim1* mRNA is up at 2 and 6 hrs following trace fear conditioning in mice (Sirri *et al*, 2010), and in rat CA1 24 hours after novel environment exposure or after fear conditioning training (Duke *et al*, 2017). The findings in rat suggest that *Hexim1* upregulation during memory formation is not species-specific. We predict that this upregulation in *Hexim1* mRNA helps neurons replenish HEXIM1 protein to baseline levels.

The role of P-TEFb regulation in neurons had not been previously explored. In this work we identified that inhibiting P-TEFb pharmacologically suppressed stimulus-dependent activation of the four IEGs we tested. This is in agreement with previously reported effects of these drugs on *Arc* and *Fos* (Saha *et al.*, 2011; Savell *et al.*, 2016), demonstrating the central role of P-TEFb activity in stimulus-dependent activation of neuronal IEGs. The dampened IEG responses after overexpression of HEXIM1 or HMBA treatment demonstrate that HEXIM1 is a critical regulator of P-TEFb-dependent responses in neurons, which maintains P-TEFb in a sequestered state allowing for optimal IEG responses to stimuli. Since we detected a decrease of HEXIM1 protein levels during recovery from an initial depolarization, we speculate that normal sequestration of P-TEFb is impaired. Indeed, we observed dampened responses for some genes to a subsequent stimulation for several hours after the initial stimulation.

Interestingly, repeated stimulation on the same day tends to re-activate gene expression in the same ensemble of neurons in the hippocampus (Cai *et al*, 2016). Thus, how neurons alter their gene transcription programs in response to multiple stimuli occurring temporally close together is critical for understanding neuroplasticity. However, like others have observed (Guzowski *et al*, 2006; Rienecker *et al.*, 2022), we see that transcriponal responses of IEGs are impaired for at time after a prior stimuli. For *Fos* and *Egr1*, recovery from a prior stimulation takes several hours, and we implicate HEXIM1 and P-TEFb in this dampened transcriptional response. However, other genes recover more quickly. For example, despite initial dampened responses, *Nr4a2* had no significant dampening of stimulation with 2 hrs of recovery. Its expression (without KCl stimulation) also seems to have a different sensitivity to HMBA than the other IEGs tested, suggesting it may have a different sensitivity to HEXIM1/P-TEFb regulation at baseline compared to other genes. *Arc* also recovered very quickly, and surprisingly had an even stronger induction to a second KCl stimulation after a 4 hr recovery, perhaps suggesting it employs an alternative mechanism for recovery of inducibility relative to other genes. Based on these combined findings, we hypothesize that early dampening of *Arc* expression after the initial stimulation is quickly reset to promote an even more robust activation within a few hours of

the initial stimulation.

There may be correlates between this recovery timeline and capacity to learn. For example, massed training paradigms with less than 1 hr. intervals between training session show impaired long-term learning compared to intervals spread out across days (Commins *et al*, 2003; Mastrorilli *et al*, 2022). However, intervals of several hours on the same day show long-term memory enhancement (Cai *et al.*, 2016; Yetton *et al*, 2019). This coincides roughly with our findings that following a 4 hr recovery, neurons are recovering *Fos* and *Egr1* inducibility and *Arc* induction is enhanced. Further work is required to determine if these transcriptional changes underlie improved plasticity and memory at these timescales.

In conclusion, *HEXIM1* mRNA exhibits strong correlations with poorer cognition in Alzheimer's disease, with particular associations observed in neurons. This highlighted the need to better understand its role in inducible gene expression in neurons. Importantly, we find that the HEXIM1 protein supports poising of IEGs at baseline so they may respond strongly and quickly to stimuli. This is a critical first step in understanding the molecular function of HEXIM1 in regulating the expression of memory-associated genes in neurons.

METHODS

Bulk RNA-seq. RNA-seq data was sourced from the ROS/MAP longitudinal study and autopsy. Data sets include the caudate nucleus (CN), dorsolateral prefrontal cortex (DLPFC), and posterior cingulate cortex (PCC). To evaluate the data, a multiple linear regression model (cross-sectional and AD-related pathology) as well as a linear mixed-effects model (longitudinal) was used. Covariates: Age at Death, Sex, Post-Mortem Interval (PMI), Interval Death, Latency to Death. Number of subjects and demographic information for this analysis is detailed in **Supplementary Table 1**.

snRNA-seq. snRNA-seq data was sourced from the ROS/MAP longitudinal study and autopsy. 299 individuals with normal cognition (n= 142, cogdx = 1 at initial clinic visit) or AD dementia (n= 157, cogdx =4 or 5 at initial clinic visit) were analyzed. Negative binomial lognormal mixed models implemented in the NEBULA R package (v1.2.0) were used for this analysis, with the model "count matrix ~ sex + age_death + pmi + clinical group". Genes with expressions in minimum 10% of all cells were used for the model. Cells were removed if they counted more than 20,000 or less than 200 total RNA UMIs, or had more than 5% mitochondrially mapped reads. The gene count matrix input of the model was the UMI count data from RNA assay normalized and scaled by "sctransform" R package (https://github.com/satijalab/sctransform). NEBULA-HL method is used for the modeling. The p value calculated from the models was FDR adjusted using R function "p.adjust" using "BH" as the method.

Animals. C57BL/6J mice were purchased from Envigo or the Jackson Laboratory. Mice were group housed, kept under 12:12 light/dark cycles, with food and water available *ad libitum*. All procedures were approved by the Vanderbilt or Loyola Institutional Animal Care and Use Committees and conducted in full compliance with the Association for Assessment and Accreditation of Laboratory Animal Care (AAALAC).

Cell Culture. Primary neuron cultures were made from neonatal (P0) mice. Dissected hippocampi were treated with papain, supplemented with cysteine, and triturated to dissociate neurons in neurobasal complete media (neurobasal with 1× B27 supplement, 1 mM sodium pyruvate, 1 mM HEPES, 100 U/mL penicillin, 100 μg/mL streptomycin, and 0.5 mM L-glutamine) plus

10% fetal bovine serum (FBS). Cells were passed through a 100-µm filter (Falcon) and plated in neurobasal complete media without FBS. On day *in vitro* 1 (DIV 1), media was again changed to neurobasal complete without FBS, and ½ the media was changed every 2-3 days thereafter. All primary neuron experiments were performed using neurons at DIV 12–15. Biological replicates were made from different preparations of primary neurons.

Neuro-2a (N2a) cells (CCL-131) were obtained from ATCC and maintained according to their recommended conditions. To differentiate N2a, cells were attached overnight in growth media, then media was changed to differentiation media (DMEM with L-glutamine without glucose, 10 mM galactose, 100 U/mL penicillin, 100 µg/mL streptomycin, and 1× N2 supplement). After 2 days, media was changed to neurobasal complete media. For drug/KCl studies, cells were incubated in neurobasal overnight prior to the application of drug or KCl. For the restimulation time course study, KCl was applied at least 1 hr. after switching to neurobasal complete for the 24 hr. washout time point, then the subsequent time points occurred on the next day. Biological replicates of N2a cells were prepared from different passages of the cell line.

RT-PCR. Total RNA was extracted from samples using RNeasy Plus Mini kit (QIAGEN) and eluted in 30–50 µl of RNase free water. Sample concentration and purity were analyzed using a NanoDrop One Microvolume UV-Vis Spectrophotometer (Thermo Scientific) and cDNA synthesis was conducted in 10-µl reaction using SuperScript VILO master mix (Invitrogen) according to manufacturer instructions. All cDNA reactions were diluted 1:10 with RNase-free water. RT-PCR was performed on a BioRad CFX96 or Opus CFX384 RT-PCR detection system in 10-15-µl reactions containing SsoAdvanced Universal SYBR Green Supermix and 250 µM primer and 3-4.5 µl of diluted cDNA. Relative fold quantification of gene expression between samples was calculated using the comparative C_t method (Livak & Schmittgen, 2001) and normalized to *Hypoxanthine phosphoribosyltransferase* (*Hprt*). Each experiment was run as 2-3 technical replicates, and the average of the technical replicates is reported for each datapoint as an individual biological replicate. To ensure we only used data from neurons that were healthy enough to robustly activate IEGs, RT-PCR was only included in the final analysis if *Fos* and *Egr1* mRNAs were induced at least 2-fold by KCl in control conditions. This criterion led to the exclusion of seven biological replicates across our in vitro studies.

Gene and primer direction	**Sequence (5' to 3')**
Hprt-f	GGAGTCCTGTTGATGTTGCCAGTA
Hprt-r	GGGACGCAGCAACTGACATTTCTA
Egr1-f	AGCGCCTTCAATCCTCAAG
Egr1-r	TTTGGCTGGGATAACTCGTC
Egr1-pre-mRNA-f	CATCGGGAGTCAGTGGTAGC
Egr1-pre-mRNA -r	AGGGAGAAGCGGCCAGTATA
Fos-f	TACTACCATTCCCCAGCCGA
Fos-r	GCGCAAAAGTCCTGTGTGTT
Fos- pre-mRNA-f	GCAAATCACACTCTGCCTGC
Fos-pre-mRNA-r	GCTGCAGCCATCTTATTCCG
Hexim1-f	CCTGATCTCAAAACCGGCCT

Hexim1-r	AATCCTCATCGCTGGTGTCG
Arc-f	ACGATCTGGCTTCCTCATTCTGCT
Arc-r	AGGTTCCCTCAGCATCTCTGCTTT
Arc-pre-mRNA-f	ACAGGAAGCAGCAAGATGGT
Arc-pre-mRNA-r	ACAGAGCCAGGAGAATGACAC
Nr4a2-f	AGCCACCTTGCTTGTACCAAATGC
Nr4a2-r	TTGTAGTAAACCGACCCGCTGTGT
Nr4a2-pre-mRNA-f	GTCTCCTGAAAACCTGCCCA
Nr4a2-pre-mRNA-r	AGCCCACGTCGATTCCAATC

Immunocytochemistry (ICC). Cells were plated on PDL-coated cover slips, rinsed twice in ice chilled 1xPBS, and cross-linked in 4% PFA (diluted in 1xPBS) for 15 minutes at room temperature. Cells were blocked and permeabilized in 10% goat serum and 0.3% TritonX-100 in 1xPBS for 1 hr at room temperature. Primary antibodies were added to cells in binding buffer (3.3% goat serum and 0.1% TritonX-100 in 1xPBS). Cells were washed three times in the same buffer used with the primary antibodies. Secondary antibodies were applied in binding buffer for 1 hr. at room temperature, and washed three times in the same. Cells were washed one time in 1xPBS before mounting in DAPI containing ProLong Gold Antifade mounting solution. Slides were dried overnight, images were acquired using a IX73 microscope (Olympus) and cellSens standard software.

KCl treatments. KCl was prepared in water and sterile filtered. Stimulations occurred for 30 min. or 2 hrs, as indicated. Primary neurons were stimulated with 25mM and dN2a were stimulated with 50mM KCl. KCl was added directly to neurobasal media, and thus the indicated mM is in addition to the 5.333mM KCl present in the normal composition of neurobasal media.

Plasmids. eYFP only control and hSyn1:F:*Hexim1* expression vectors were cloned into the AAV-shRNA-ctrl backbone (Yu *et al*, 2015). AAV-shRNA-ctrl was a gift from Hongjun Song (Addgene plasmid # 85741). The region containing the U6 promoter and shRNA were deleted from both constructs. Whole plasmid sequencing data was conducted to validate sequences (supplementary files: wholeplasmidsequencingresults_ControlAAVplasmid.fasta and wholeplasmidsequencingresults_hSyn1Hexim1AAVplasmid.fasta).

AAV generation and treatment. Virus was produced using Helper Free Expression System and the 293AAV cell line (Cell Biolabs, Inc.). The cell pellet was lysed by alternating freeze thaw cycles in ethanol/dry ice bath three times. The supernatant was saved, and pellet was additionally extracted with Takara AAV extraction solution. Separately, virus was precipitated from culture media with 10%PEG and 625mM NaCl on ice. The solutions from freeze/thaw, AAV extraction, and the PEG pellet resuspension were combined and purified using iodixanol ultracentrifugation and were concentrated. The viral titer was determined by standard qPCR with the BioRad SYBR Green supermix using serial dilutions of the AAV backbone vector, and was concentrated to greater than 1e12 genome copies/mL. 0.3-1uL of virus was applied to cells in 500uL of culture medium 1 week prior to harvesting RNA.

Live cell imaging. Cells were imaged with ZOE Florescent Cell Imager (BioRad) 1 week after

transduction with AAV.

Inhibitors. Inhibitors employed in this study were: DRB (Cayman Chemical, 10010302), FLAVO (Selleckchem, S1230, Batch S123007), and HMBA (Sigma, lot MKCN8312). DRB applied at dose of 25uM in primary neurons and 50uM in dN2a. FLAVO was used at 100nM and HMBA at 20mM in all cell types. Cells were pretreated with DRB and FLAVO for 30 min for primary neurons and 30 min to overnight in dN2a. Cells were pretreated with HMBA 1 hr. prior to KCl treatment.

Western blots. SDS-PAGE was conducted in 4-20% polyacrylamide gels. Secondary antibodies were goat anti-mouse infrared (IR) 680 (LI-COR Biosciences; #926-68020), goat anti-mouse IR 800 (LI-COR Biosciences; #926-32210), and goat anti-rabbit IR 800 (LI-COR Biosciences; #925-32211). Secondaries used for CoIP were specific to the light chain (Jackson ImmunoResearch). Membranes were imaged on the LI-COR Biosciences Odyssey fluorescence imaging system.

Co-Immunoprecipitation. Two hippocampi were homogenized using a pellet pestle motor and dounce homogenization in 400 µL of lysis buffer consisting of the following reagents: 150 mM NaCl, 50 mM Tris-HCl, 1% NP-40, 5 mM EDTA, 1 mM DTT, Phosphatase inhibitor (Thermo-Scientific, Inc.) 1X EDTA-Free, 200 µM PMSF, 0.1 µM MLR and 1x NaF. The lysate was centrifuged at 12,000xg for 10 min at 4C. The supernatant was then divided into 3 fractions of 100 µL for IgG, HEXIM1 and CDK9 Co-IPs and 1 fraction of 60 µL was saved for the input sample. An equal mix of protein A and protein G dynabeads (Invitrogen) were washed before use 3 times with Immunoprecipitation (IP) buffer consisting of 150 mM NaCl, 50 mM Tris-HCl, 0.5% NP-40 and phosphatase inhibitor 1X EDTA-Free and then we added 1 µL of the individual antibody to 10 µL of the beads. The beads with the antibody and the supernatant fraction were placed in a tube rotator at 4°C for 1 hr. Then, the samples washed 5 times with IP buffer using a magnetic rack. The proteins were eluted at 65°C for 5 min in agitation with 2x sample buffer (250 mM Tris-HCl pH 8, 40% glycerol, 10 mM EDTA, 8% SDS, 400 mM DTT and 0.05% bromophenol blue). These samples were directly loaded into the SDS-PAGE for Western blot analysis.

Antibodies.

Antigen	Company	Source	Dilution	Catalogue	Lot	Iso-type
HEXIM1	abcam	Rabbit	1:1000 (WB/ICC)	ab25388 1mg/mL	GR3245992-1 GR3460630-1	IgG
Beta-ACTIN	Cell Signaling	Mouse	1:2000 (WB)	8H10D10	21	IgG2b
Cdk9	abcam	Rabbit monoclonal	1:1000 (WB)	ab239364	1023428-1	IgG
Tubulin, beta III (Tuj1)	Millipore	mouse	1:2000 (ICC)	TU-20, MAB1637	3407183	IgG1
GAPDH	Abcam	Mouse monoclonal	1:2000 (WB)	ab8245	1035914-4	IgG1

Rabbit IgG	Ther-mofisher	Rabbit	NA	02-6102	SJ257848	IgG

ACKNOWLEDGEMENTS. This study is supported by NIH grants K01 MH129760 to CBG, R01 MH057014 to RJC, T32 MH065215 to RJC, R01 AG074012 to TJH, R01 AG061518 to TJH, and R01 AG059716 to TJH. We thank Hero Haji for her help with cloning and Eugenia V. Gurevich for help with virus generation.

CONFLICT OF INTEREST

TJH serves on the scientific advisory board for Vivid Genomics and as Deputy Editor for A&D: TRCI.

REFERENCES

Alazami AM, Al-Owain M, Alzahrani F, Shuaib T, Al-Shamrani H, Al-Falki YH, Al-Qahtani SM, Alsheddi T, Colak D, Alkuraya FS (2012) Loss of function mutation in LARP7, chaperone of 7SK ncRNA, causes a syndrome of facial dysmorphism, intellectual disability, and primordial dwarfism. *Hum Mutat* 33: 1429-1434

Alberini CM, Kandel ER (2014) The regulation of transcription in memory consolidation. *Cold Spring Harb Perspect Biol* 7: a021741

Athaide Rocha KM, Machado FR, Poetini M, Giacomeli R, Boeira SP, Jesse CR, Gomes de Gomes M (2023) Assessment of suberoylanilide hydroxamic acid on a Alzheimer's disease model induced by beta-amyloid((1-42)) in aged female mice: Neuromodulatory and epigenetic effect. *Chem Biol Interact* 375: 110429

Badrikoohi M, Esmaeili-Bandboni A, Babaei P (2022) Simultaneous administration of bromodomain and histone deacetylase I inhibitors alleviates cognition deficit in Alzheimer's model of rats. *Brain Res Bull* 179: 49-56

Barrandon C, Bonnet F, Nguyen VT, Labas V, Bensaude O (2007) The transcription-dependent dissociation of P-TEFb-HEXIM1-7SK RNA relies upon formation of hnRNP-7SK RNA complexes. *Mol Cell Biol* 27: 6996-7006

Baumli S, Endicott JA, Johnson LN (2010) Halogen bonds form the basis for selective P-TEFb inhibition by DRB. *Chem Biol* 17: 931-936

Benito E, Ramachandran B, Schroeder H, Schmidt G, Urbanke H, Burkhardt S, Capece V, Dean C, Fischer A (2017) The BET/BRD inhibitor JQ1 improves brain plasticity in WT and APP mice. *Transl Psychiatry* 7: e1239

Bennett DA, Schneider JA, Buchman AS, Mendes de Leon C, Bienias JL, Wilson RS (2005) The Rush Memory and Aging Project: study design and baseline characteristics of the study cohort. *Neuroepidemiology* 25: 163-175

Cai DJ, Aharoni D, Shuman T, Shobe J, Biane J, Song W, Wei B, Veshkini M, La-Vu M, Lou J *et al* (2016) A shared neural ensemble links distinct contextual memories encoded close in time. *Nature* 534: 115-118

Canchi S, Raao B, Masliah D, Rosenthal SB, Sasik R, Fisch KM, De Jager PL, Bennett DA, Rissman RA (2019) Integrating Gene and Protein Expression Reveals Perturbed Functional Networks in Alzheimer's Disease. *Cell Rep* 28: 1103-1116 e1104

Chao SH, Price DH (2001) Flavopiridol inactivates P-TEFb and blocks most RNA polymerase II transcription in vivo. *J Biol Chem* 276: 31793-31799

Chen YA, Lu CH, Ke CC, Chiu SJ, Chang CW, Yang BH, Gelovani JG, Liu RS (2021) Evaluation of Class IIa Histone Deacetylases Expression and In Vivo Epigenetic Imaging in a Transgenic Mouse Model of Alzheimer's Disease. *Int J Mol Sci* 22

Choi H, Kim C, Song H, Cha MY, Cho HJ, Son SM, Kim HJ, Mook-Jung I (2019) Amyloid beta-induced elevation of O-GlcNAcylated c-Fos promotes neuronal cell death. *Aging Cell* 18: e12872

Clayton DF (2000) The genomic action potential. *Neurobiol Learn Mem* 74: 185-216

Commins S, Cunningham L, Harvey D, Walsh D (2003) Massed but not spaced training impairs spatial memory. *Behav Brain Res* 139: 215-223

Contreras X, Barboric M, Lenasi T, Peterlin BM (2007) HMBA releases P-TEFb from HEXIM1 and 7SK snRNA via PI3K/Akt and activates HIV transcription. *PLoS Pathog* 3: 1459-1469

Cubelos B, Sebastian-Serrano A, Beccari L, Calcagnotto ME, Cisneros E, Kim S, Dopazo A, Alvarez-Dolado M, Redondo JM, Bovolenta P *et al* (2010) Cux1 and Cux2 regulate dendritic branching, spine morphology, and synapses of the upper layer neurons of the cortex. *Neuron* 66: 523-535
De Jager PL, Ma Y, McCabe C, Xu J, Vardarajan BN, Felsky D, Klein HU, White CC, Peters MA, Lodgson B *et al* (2018) A multi-omic atlas of the human frontal cortex for aging and Alzheimer's disease research. *Sci Data* 5: 180142
Desjardins S, Mayo W, Vallee M, Hancock D, Le Moal M, Simon H, Abrous DN (1997) Effect of aging on the basal expression of c-Fos, c-Jun, and Egr-1 proteins in the hippocampus. *Neurobiol Aging* 18: 37-44
Duke CG, Kennedy AJ, Gavin CF, Day JJ, Sweatt JD (2017) Experience-dependent epigenomic reorganization in the hippocampus. *Learn Mem* 24: 278-288
Espana J, Valero J, Minano-Molina AJ, Masgrau R, Martin E, Guardia-Laguarta C, Lleo A, Gimenez-Llort L, Rodriguez-Alvarez J, Saura CA (2010) beta-Amyloid disrupts activity-dependent gene transcription required for memory through the CREB coactivator CRTC1. *J Neurosci* 30: 9402-9410
Faraji N, Badrikoohi M, Babaei P (2023) Effect of BRD4 Inhibitor on Cognitive Deficit and c-Fos /BDNF level in rats with Alzheimer's disease. *Neuroscience and Behavioral Physiology* 53: 678-687
Fleischmann A, Hvalby O, Jensen V, Strekalova T, Zacher C, Layer LE, Kvello A, Reschke M, Spanagel R, Sprengel R *et al* (2003) Impaired long-term memory and NR2A-type NMDA receptor-dependent synaptic plasticity in mice lacking c-Fos in the CNS. *J Neurosci* 23: 9116-9122
Francis YI, Fa M, Ashraf H, Zhang H, Staniszewski A, Latchman DS, Arancio O (2009) Dysregulation of histone acetylation in the APP/PS1 mouse model of Alzheimer's disease. *J Alzheimers Dis* 18: 131-139
Fujinaga K, Barboric M, Li Q, Luo Z, Price DH, Peterlin BM (2012) PKC phosphorylates HEXIM1 and regulates P-TEFb activity. *Nucleic Acids Res* 40: 9160-9170
Greer CB, Tanaka Y, Kim YJ, Xie P, Zhang MQ, Park IH, Kim TH (2015) Histone Deacetylases Positively Regulate Transcription through the Elongation Machinery. *Cell Rep* 13: 1444-1455
Grimm R, Schicknick H, Riede I, Gundelfinger ED, Herdegen T, Zuschratter W, Tischmeyer W (1997) Suppression of c-fos induction in rat brain impairs retention of a brightness discrimination reaction. *Learn Mem* 3: 402-413
Guzowski JF, Lyford GL, Stevenson GD, Houston FP, McGaugh JL, Worley PF, Barnes CA (2000) Inhibition of activity-dependent arc protein expression in the rat hippocampus impairs the maintenance of long-term potentiation and the consolidation of long-term memory. *J Neurosci* 20: 3993-4001
Guzowski JF, Miyashita T, Chawla MK, Sanderson J, Maes LI, Houston FP, Lipa P, McNaughton BL, Worley PF, Barnes CA (2006) Recent behavioral history modifies coupling between cell activity and Arc gene transcription in hippocampal CA1 neurons. *Proc Natl Acad Sci U S A* 103: 1077-1082
Guzowski JF, Setlow B, Wagner EK, McGaugh JL (2001) Experience-dependent gene expression in the rat hippocampus after spatial learning: a comparison of the immediate-early genes Arc, c-fos, and zif268. *J Neurosci* 21: 5089-5098

Jang MK, Mochizuki K, Zhou M, Jeong HS, Brady JN, Ozato K (2005) The bromodomain protein Brd4 is a positive regulatory component of P-TEFb and stimulates RNA polymerase II-dependent transcription. *Mol Cell* 19: 523-534
Kaczmarek L (2000) Gene expression in learning processes. *Acta Neurobiol Exp (Wars)* 60: 419-424
Kennedy AJ, Rahn EJ, Paulukaitis BS, Savell KE, Kordasiewicz HB, Wang J, Lewis JW, Posey J, Strange SK, Guzman-Karlsson MC *et al* (2016) Tcf4 Regulates Synaptic Plasticity, DNA Methylation, and Memory Function. *Cell Rep* 16: 2666-2685
Kilgore M, Miller CA, Fass DM, Hennig KM, Haggarty SJ, Sweatt JD, Rumbaugh G (2010) Inhibitors of class 1 histone deacetylases reverse contextual memory deficits in a mouse model of Alzheimer's disease. *Neuropsychopharmacology* 35: 870-880
Kim YJ, Greer CB, Cecchini KR, Harris LN, Tuck DP, Kim TH (2013) HDAC inhibitors induce transcriptional repression of high copy number genes in breast cancer through elongation blockade. *Oncogene* 32: 2828-2835
Krueger BJ, Jeronimo C, Roy BB, Bouchard A, Barrandon C, Byers SA, Searcey CE, Cooper JJ, Bensaude O, Cohen EA *et al* (2008) LARP7 is a stable component of the 7SK snRNP while P-TEFb, HEXIM1 and hnRNP A1 are reversibly associated. *Nucleic Acids Res* 36: 2219-2229
Leggio GM, Catania MV, Puzzo D, Spatuzza M, Pellitteri R, Gulisano W, Torrisi SA, Giurdanella G, Piazza C, Impellizzeri AR *et al* (2016) The antineoplastic drug flavopiridol reverses memory impairment induced by Amyloid-ss1-42 oligomers in mice. *Pharmacol Res* 106: 10-20
Livak KJ, Schmittgen TD (2001) Analysis of relative gene expression data using real-time quantitative PCR and the 2(-Delta Delta C(T)) Method. *Methods* 25: 402-408
Lu H, Xue Y, Yu GK, Arias C, Lin J, Fong S, Faure M, Weisburd B, Ji X, Mercier A *et al* (2015) Compensatory induction of MYC expression by sustained CDK9 inhibition via a BRD4-dependent mechanism. *Elife* 4: e06535
Magistri M, Velmeshev D, Makhmutova M, Patel P, Sartor GC, Volmar CH, Wahlestedt C, Faghihi MA (2016) The BET-Bromodomain Inhibitor JQ1 Reduces Inflammation and Tau Phosphorylation at Ser396 in the Brain of the 3xTg Model of Alzheimer's Disease. *Curr Alzheimer Res* 13: 985-995
Marcus DL, Strafaci JA, Miller DC, Masia S, Thomas CG, Rosman J, Hussain S, Freedman ML (1998) Quantitative neuronal c-fos and c-jun expression in Alzheimer's disease. *Neurobiol Aging* 19: 393-400
Marie IJ, Chang HM, Levy DE (2018) HDAC stimulates gene expression through BRD4 availability in response to IFN and in interferonopathies. *J Exp Med* 215: 3194-3212
Marshall NF, Price DH (1995) Purification of P-TEFb, a transcription factor required for the transition into productive elongation. *J Biol Chem* 270: 12335-12338
Mastrorilli V, Centofante E, Antonelli F, Rinaldi A, Mele A (2022) The neural substrate of spatial memory stabilization depends on the distribution of the training sessions. *Proc Natl Acad Sci U S A* 119: e2120717119
Mathys H, Boix CA, Akay LA, Xia Z, Davila-Velderrain J, Ng AP, Jiang X, Abdelhady G, Galani K, Mantero J *et al* (2024) Single-cell multiregion dissection of Alzheimer's disease. *Nature*

Mathys H, Davila-Velderrain J, Peng Z, Gao F, Mohammadi S, Young JZ, Menon M, He L, Abdurrob F, Jiang X *et al* (2019) Single-cell transcriptomic analysis of Alzheimer's disease. *Nature* 570: 332-337
Medina AC, Torres-Garcia ME, Rodriguez-Serrano LM, Bello-Medina PC, Quirarte GL, McGaugh JL, Prado-Alcala RA (2019) Inhibition of transcription and translation in dorsal hippocampus does not interfere with consolidation of memory of intense training. *Neurobiol Learn Mem* 166: 107092
Myrum C, Moreno-Castilla P, Rapp PR (2022) 'Arc'-hitecture of normal cognitive aging. *Ageing Res Rev* 80: 101678
Ni W, Zhang F, Zheng L, Wang L, Liang Y, Ding Y, Yik JHN, Haudenschild DR, Fan S, Hu Z (2020) Cyclin-Dependent Kinase 9 (CDK9) Inhibitor Atuveciclib Suppresses Intervertebral Disk Degeneration via the Inhibition of the NF-kappaB Signaling Pathway. *Front Cell Dev Biol* 8: 579658
Nikkar R, Esmaeili-Bandboni A, Badrikoohi M, Babaei P (2022) Effects of inhibiting astrocytes and BET/BRD4 chromatin reader on spatial memory and synaptic proteins in rats with Alzheimer's disease. *Metab Brain Dis* 37: 1119-1131
Pang C, Yang H, Hu B, Wang S, Chen M, Cohen DS, Chen HS, Jarrell JT, Carpenter KA, Rosin ER *et al* (2019) Identification and Analysis of Alzheimer's Candidate Genes by an Amplitude Deviation Algorithm. *J Alzheimers Dis Parkinsonism* 9
Park S, Oh S, Kim N, Kim EK (2023) HMBA ameliorates obesity by MYH9- and ACTG1-dependent regulation of hypothalamic neuropeptides. *EMBO Mol Med* 15: e18024
Rienecker KDA, Poston RG, Saha RN (2020) Merits and Limitations of Studying Neuronal Depolarization-Dependent Processes Using Elevated External Potassium. *ASN Neuro* 12: 1759091420974807
Rienecker KDA, Poston RG, Segales JS, Finholm IW, Sono MH, Munteanu SJ, Ghaninejad-Esfahani M, Rejepova A, Tejeda-Garibay S, Wickman K *et al* (2022) Mild membrane depolarization in neurons induces immediate early gene transcription and acutely subdues responses to a successive stimulus. *J Biol Chem* 298: 102278
Saha RN, Wissink EM, Bailey ER, Zhao M, Fargo DC, Hwang JY, Daigle KR, Fenn JD, Adelman K, Dudek SM (2011) Rapid activity-induced transcription of Arc and other IEGs relies on poised RNA polymerase II. *Nat Neurosci* 14: 848-856
Sanchez GJ, Richmond PA, Bunker EN, Karman SS, Azofeifa J, Garnett AT, Xu Q, Wheeler GE, Toomey CM, Zhang Q *et al* (2018) Genome-wide dose-dependent inhibition of histone deacetylases studies reveal their roles in enhancer remodeling and suppression of oncogenic super-enhancers. *Nucleic Acids Res* 46: 1756-1776
Savell KE, Gallus NV, Simon RC, Brown JA, Revanna JS, Osborn MK, Song EY, O'Malley JJ, Stackhouse CT, Norvil A *et al* (2016) Extra-coding RNAs regulate neuronal DNA methylation dynamics. *Nat Commun* 7: 12091
Schneeberger PE, Bierhals T, Neu A, Hempel M, Kutsche K (2019) de novo MEPCE nonsense variant associated with a neurodevelopmental disorder causes disintegration of 7SK snRNP and enhanced RNA polymerase II activation. *Sci Rep* 9: 12516
Shore SM, Byers SA, Dent P, Price DH (2005) Characterization of Cdk9(55) and differential regulation of two Cdk9 isoforms. *Gene* 350: 51-58
Singh MB, Sartor GC (2020) BET bromodomains as novel epigenetic targets for brain health and disease. *Neuropharmacology* 181: 108306

Sirri A, Bianchi V, Pelizzola M, Mayhaus M, Ricciardi-Castagnoli P, Toniolo D, D'Adamo P (2010) Temporal gene expression profile of the hippocampus following trace fear conditioning. *Brain Res* 1308: 14-23
Strekalova T, Zorner B, Zacher C, Sadovska G, Herdegen T, Gass P (2003) Memory retrieval after contextual fear conditioning induces c-Fos and JunB expression in CA1 hippocampus. *Genes Brain Behav* 2: 3-10
Su Q, Li T, He PF, Lu XC, Yu Q, Gao QC, Wang ZJ, Wu MN, Yang D, Qi JS (2021) Trichostatin A ameliorates Alzheimer's disease-related pathology and cognitive deficits by increasing albumin expression and Abeta clearance in APP/PS1 mice. *Alzheimers Res Ther* 13: 7
Teather LA, Packard MG, Smith DE, Ellis-Behnke RG, Bazan NG (2005) Differential induction of c-Jun and Fos-like proteins in rat hippocampus and dorsal striatum after training in two water maze tasks. *Neurobiol Learn Mem* 84: 75-84
Thut PD, Lindell TJ (1974) Alpha-amanitin inhibition of mouse brain form II ribonucleic acid polymerase and passive avoidance retention. *Mol Pharmacol* 10: 146-154
Wang BY, Zhong Y, Zhao Z, Miao Y (2014) Epigenetic suppression of hippocampal BDNF mediates the memory deficiency induced by amyloid fibrils. *Pharmacol Biochem Behav* 126: 83-89
Yang H, Kim J, Kim Y, Jang SW, Sestan N, Shim S (2020) Cux2 expression regulated by Lhx2 in the upper layer neurons of the developing cortex. *Biochem Biophys Res Commun* 521: 874-879
Yetton BD, Cai DJ, Spoormaker VI, Silva AJ, Mednick SC (2019) Human Memories Can Be Linked by Temporal Proximity. *Front Hum Neurosci* 13: 315
Yik JH, Chen R, Nishimura R, Jennings JL, Link AJ, Zhou Q (2003) Inhibition of P-TEFb (CDK9/Cyclin T) kinase and RNA polymerase II transcription by the coordinated actions of HEXIM1 and 7SK snRNA. *Mol Cell* 12: 971-982
Yu H, Su Y, Shin J, Zhong C, Guo JU, Weng YL, Gao F, Geschwind DH, Coppola G, Ming GL *et al* (2015) Tet3 regulates synaptic transmission and homeostatic plasticity via DNA oxidation and repair. *Nat Neurosci* 18: 836-843
Zalcman G, Federman N, de la Fuente V, Romano A (2015) Nuclear factor kappa B-dependent Zif268 expression in hippocampus is required for recognition memory in mice. *Neurobiol Learn Mem* 119: 10-17

FIGURE LEGENDS

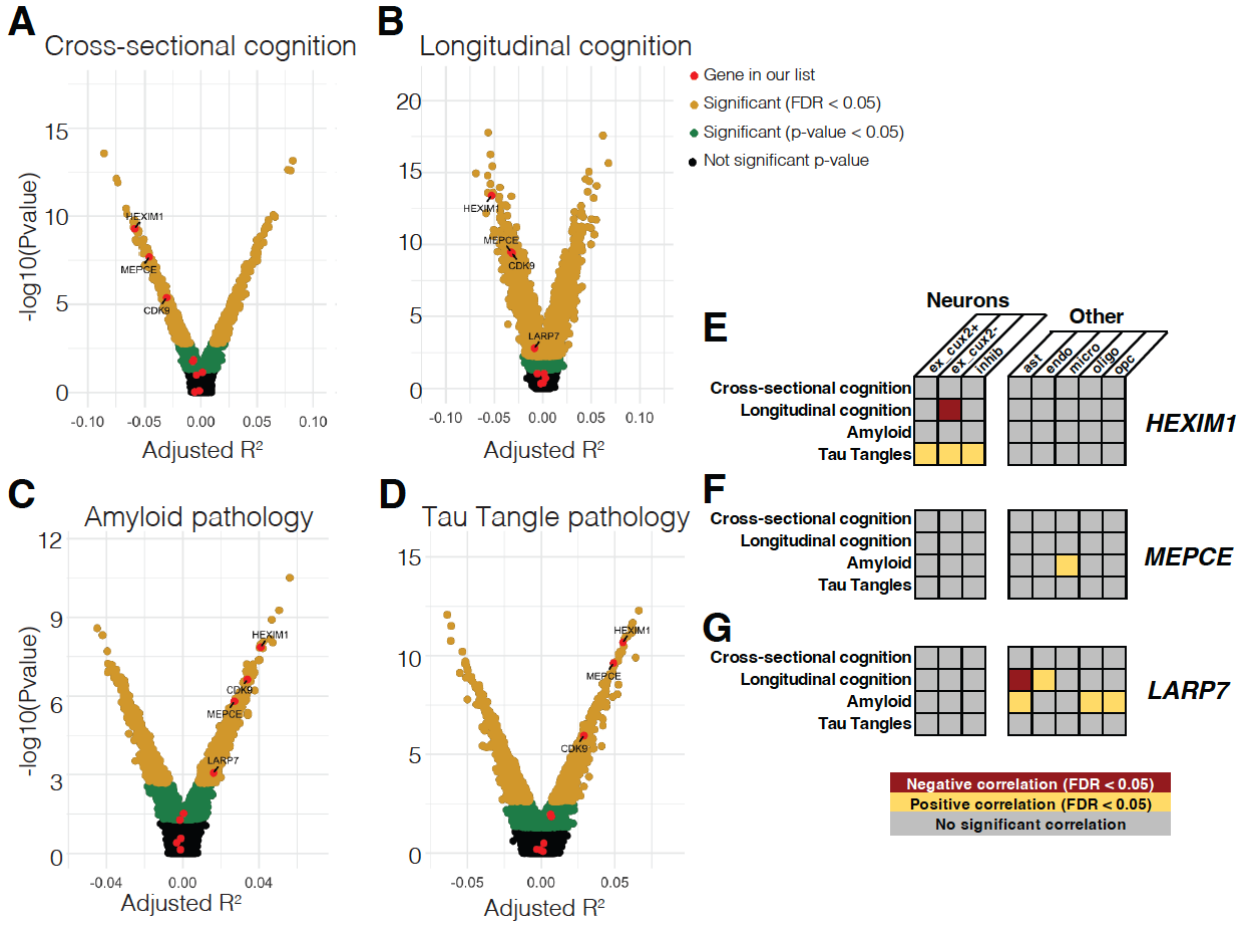

Fig. 1. Correlations between P-TEFb regulatory complex component expression and characteristics of AD in bulk and snRNA-seq. Correlations between expression of *BRD4*, *CCNT1*, *CCNT2*, *CDK9*, *HEXIM1*, *LARP7*, and *MEPCE* mRNAs and *RN7SK* non-coding RNA with **A)** cross-sectional cognition, **B)** longitudinal cognition, **C)** amyloid pathology, and **D)** tau tangle pathology in bulk tissue from the head of the caudate nucleus. Individual dots represent a single gene, and genes in the yellow region of the volcano plots are significantly correlated with the indicated pathology (FDR < 0.05). snRNA-seq correlations with AD pathologies in different cell types in DL-PFC for components of the P-TEFb inhibitory complex **E)** *HEXIM1*, **F)** *MEPCE*, and **G)** *LARP7.* ex = excitatory neurons, inhib = inhibitory neurons, ast = astrocytes, endo = endothelial cells, micro = microglia, oligo = oligodendrocytes, opc = oligodendrocyte progenitor cells.

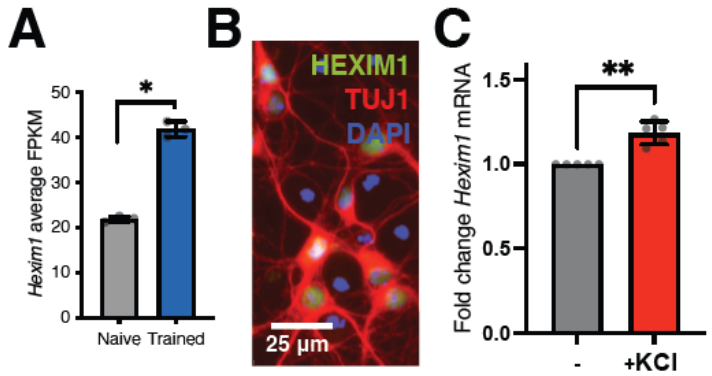

Fig. 2. HEXIM1 is an activity-dependent gene that is expressed in neurons. A) *Hexim1* expression represented as Fragments Per Kilobase of transcript per Million mapped reads (FPKM) in mouse CA1 region of hippocampus 1 hr after mild foot shock. *q (multiple hypothesis corrected p value) < 0.05. n=3 mice. **B)** ICC of HEXIM1 in mouse primary neuron culture. **C)** RT-PCR of *Hexim1* mRNA after KCl stimulation in primary neurons. n=5 biological replicates. One sample t test. **p<0.01. Error bars represent standard deviation.

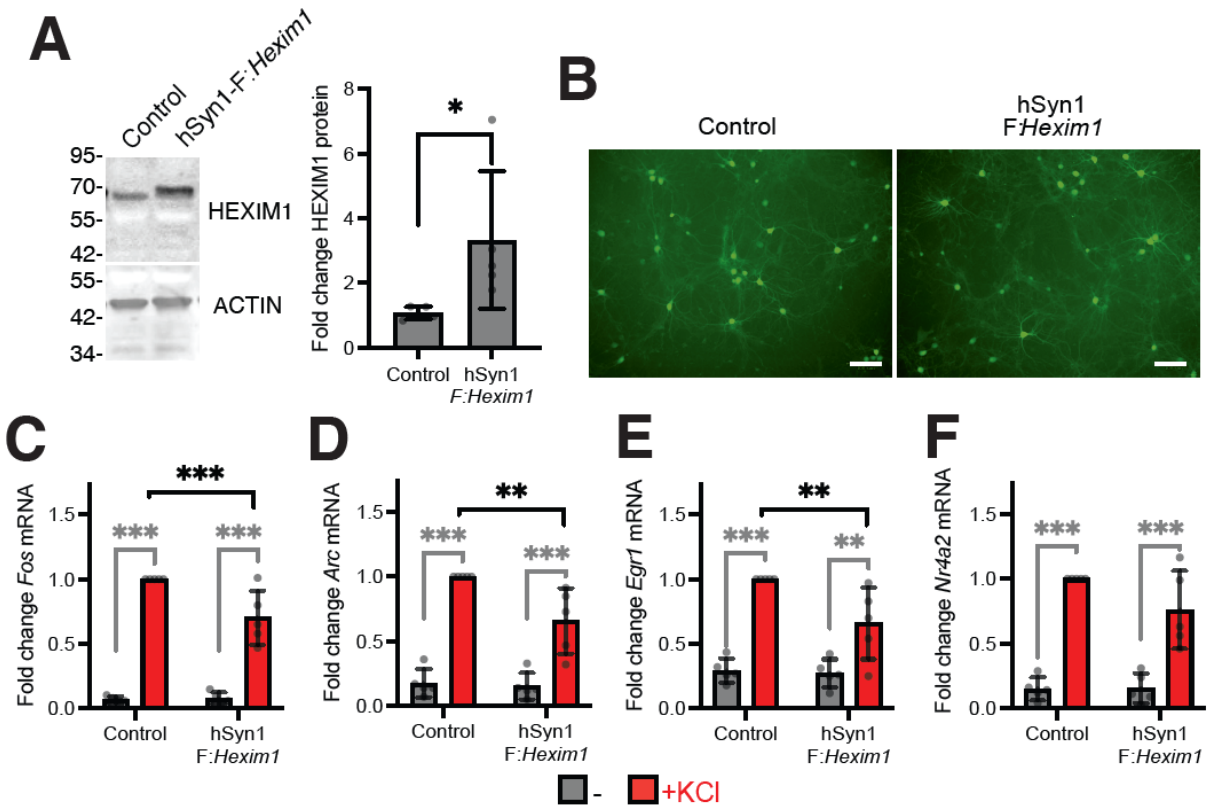

Fig. 3. Effect of HEXIM1 overexpression on IEG induction in primary neurons. A) Representative Western blot of HEXIM1 and ACTIN in whole cell lysates following Control or hSyn1-FLAG:*Hexim1* AAV9 treatment and quantitation of HEXIM1 expression changes. **B)** eYFP expression following infection with Control or hSyn1-FLAG:*Hexim1* AAV9. Scale bar = 100um. **C)** *Fos* **D)** *Arc*, **E)** *Egr1*, **F)** *Nr4a2* mRNA levels (RT-PCR) after 1-week pretreatment with virus followed by KCl stimulation in primary neurons. n=5 biological replicates. Two-way ANOVA with Sidak's multiple comparisons test. *p<0.05, **p<0.01, ***p<0.001. Error bars represent standard deviation.

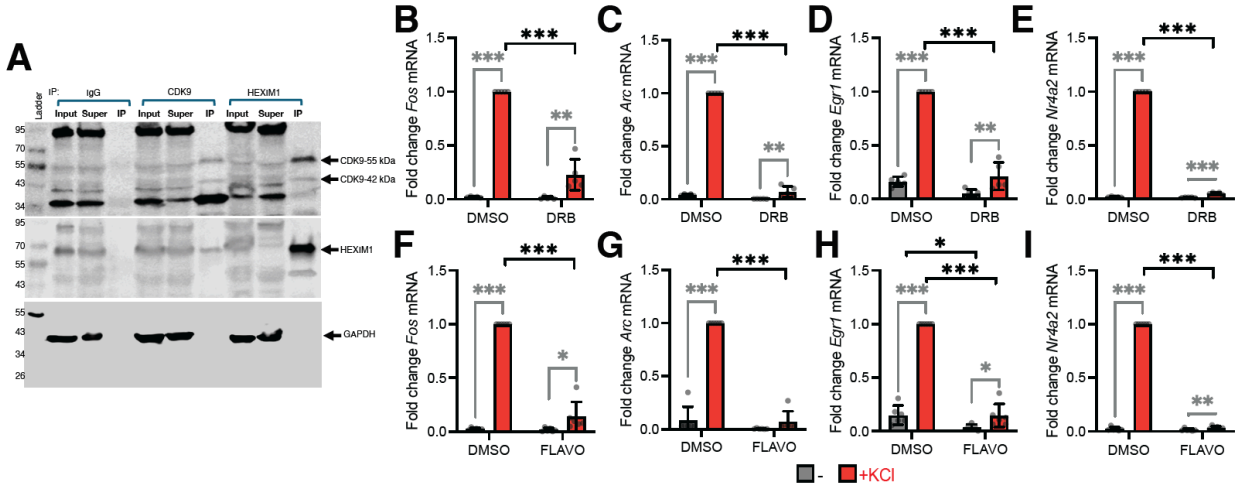

Fig. 4. HEXIM1 binds P-TEFb in the hippocampus, and P-TEFb regulates activity-dependent IEG induction in neurons. A) Coimmunoprecipitations of hippocampal lysates with HEXIM1, CDK9, and IgG antibodies. **B)** *Fos,* **C)** *Arc*, **D)** *Egr1*, **E)** *Nr4a2* mRNA levels (RT-PCR) after pretreatment with DRB followed by KCl stimulation in primary neurons. **F)** *Fos,* **G)** *Arc*, **H)** *Egr1*, **I)** *Nr4a2* mRNA levels (RT-PCR) after pretreatment with FLAVO followed by KCl stimulation in primary neurons. **B-E** n=5 biological replicates, and **F-I** n=6 biological replicates. Two-way ANOVA with Sidak's multiple comparisons test. *$p<0.05$, **$p<0.01$, ***$p<0.001$. Error bars represent standard deviation.

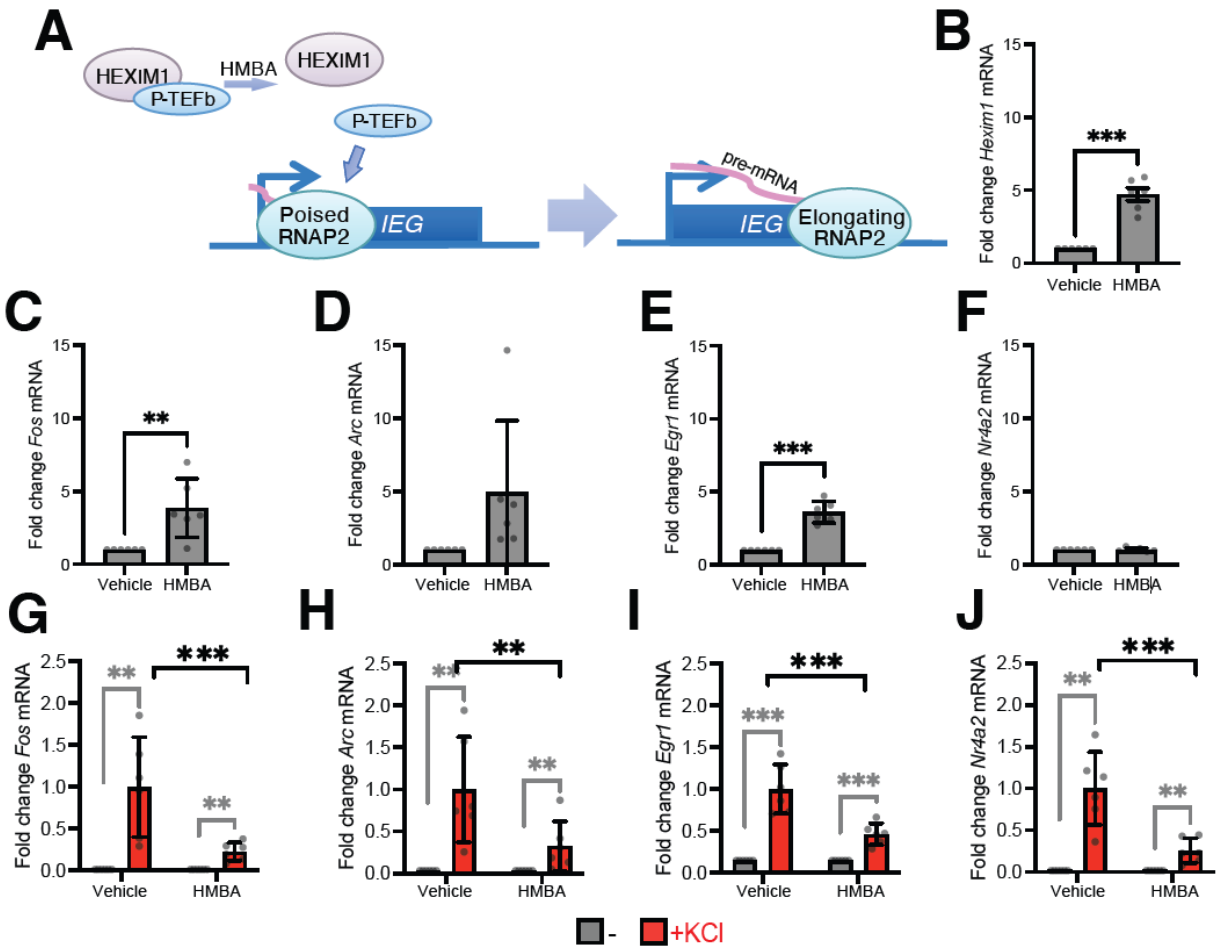

Fig. 5. Effect of disrupting HEXIM1/P-TEFb interaction with HMBA on basline and inducible gene expression in primary neurons. A) Cartoon depicting effect of HMBA on HEXIM1/P-TEFb complex. Changes in mRNA expression following HMBA treatment for **B)** *Hexim1*, **C)** *Fos*, **D)** *Arc*, **E)** *Egr1*, **F)** *Nr4a2* mRNA in primary hippocampal neurons (RT-PCR). Stimulus-dependent changes in **G)** *Fos*, **H)** *Arc*, **I)** *Egr1*, **J)** *Nr4a2* mRNA expression after HMBA followed by KCl stimulation in primary neurons. HMBA conditions were renormalized by dividing by the fold increase that HMBA caused alone to account for the baseline changes induced by HMBA. n=6 biological replicates. Two-way ANOVA with Sidak's multiple comparisons test. *p<0.05, **p<0.01, ***p<0.001. Error bars represent standard deviation.

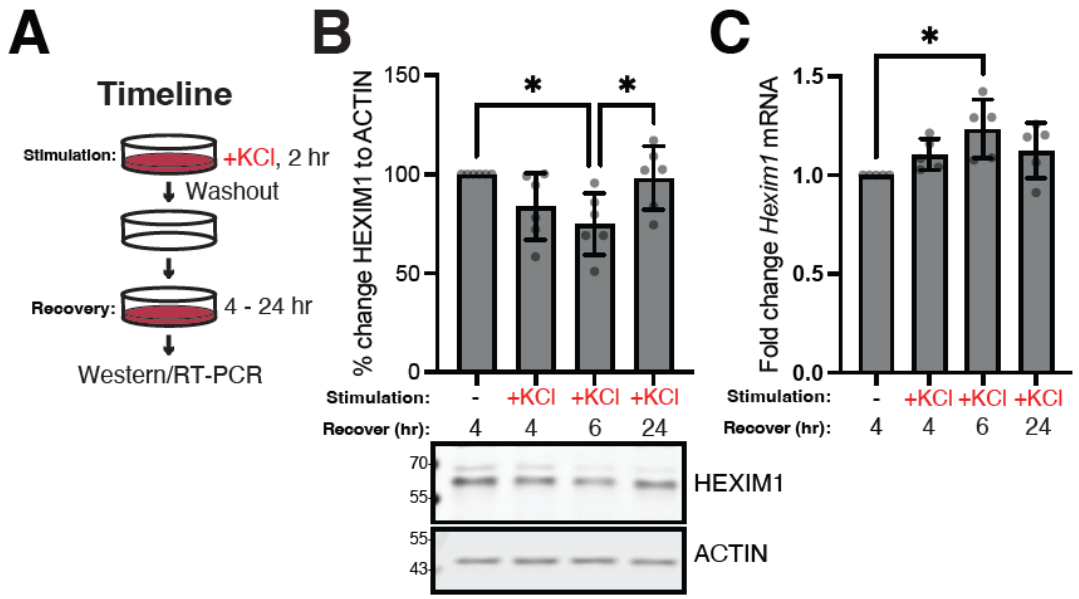

Fig. 6. HEXIM1 protein and mRNA in primary neurons following KCl stimulation. A) Timeline of KCl stimulation and recovery in **B** and **C**. **B)** Western blot quantitation of HEXIM1 relative to ACTIN during recovery after KCl in primary neuronal culture. Representative blot below. n=6 biological replicates. **C)** *Hexim1* mRNA (RT-PCR) during recovery from stimulation. One-way ANOVAs with Tukey's multiple comparisons tests. n= 5 biological replicates. *p<0.05. Error bars represent standard deviation.

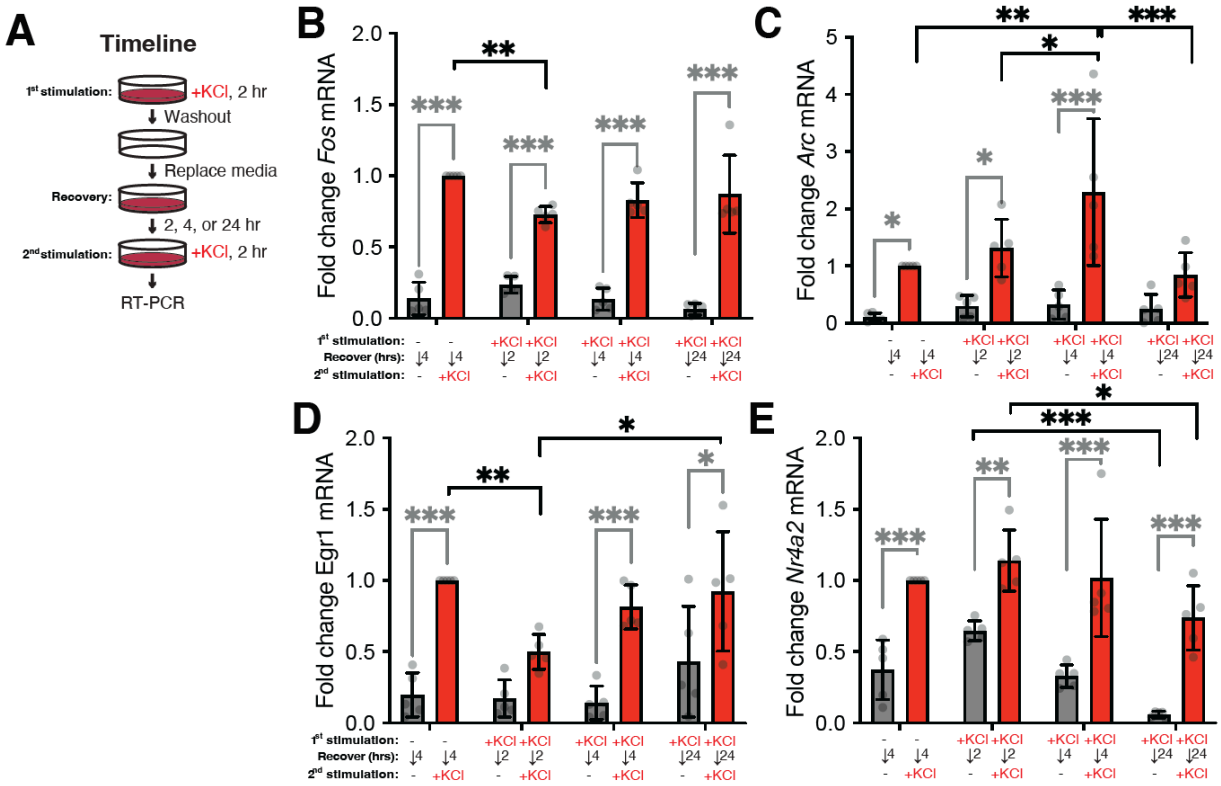

Fig. 7. Transcriptional responses of IEGs after a prior stimulation. A) Timeline of KCl stimulations in **B-E**. **B)** *Fos*, **C)** *Arc*, **D)** *Egr1*, **E)** *Nr4a2* mRNA expression (RT-PCR) in primary neurons during restimulation. n=5 biological replicates. Two-way ANOVA with Sidak's multiple comparisons test. *p<0.05, **p<0.01, ***p<0.001. Error bars represent standard deviation.

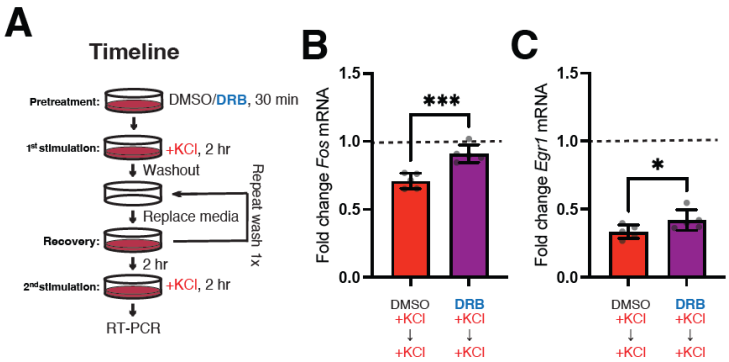

Fig. 8. Blocking P-TEFb preserves KCl induction of *Fos* and partially recovers *Egr1* inducibility during a second stimulation. A) Timeline of drug treatment and KCl stimulations in dN2a cells in **B** and **C**. B) *Fos* and C) *Egr1* mRNA (RT-PCR) after two KCl stimulations with or without DRB pretreatment. Effect of KCl alone (done at same time as the second stimulation) with no prior drug or KCl treatments was set as 1 (dashed line). n=5 biological replicates. Paired t test. * = $p < 0.05$. Error bars represent standard deviation.

SUPPLEMENTARY FIGURE LEGENDS

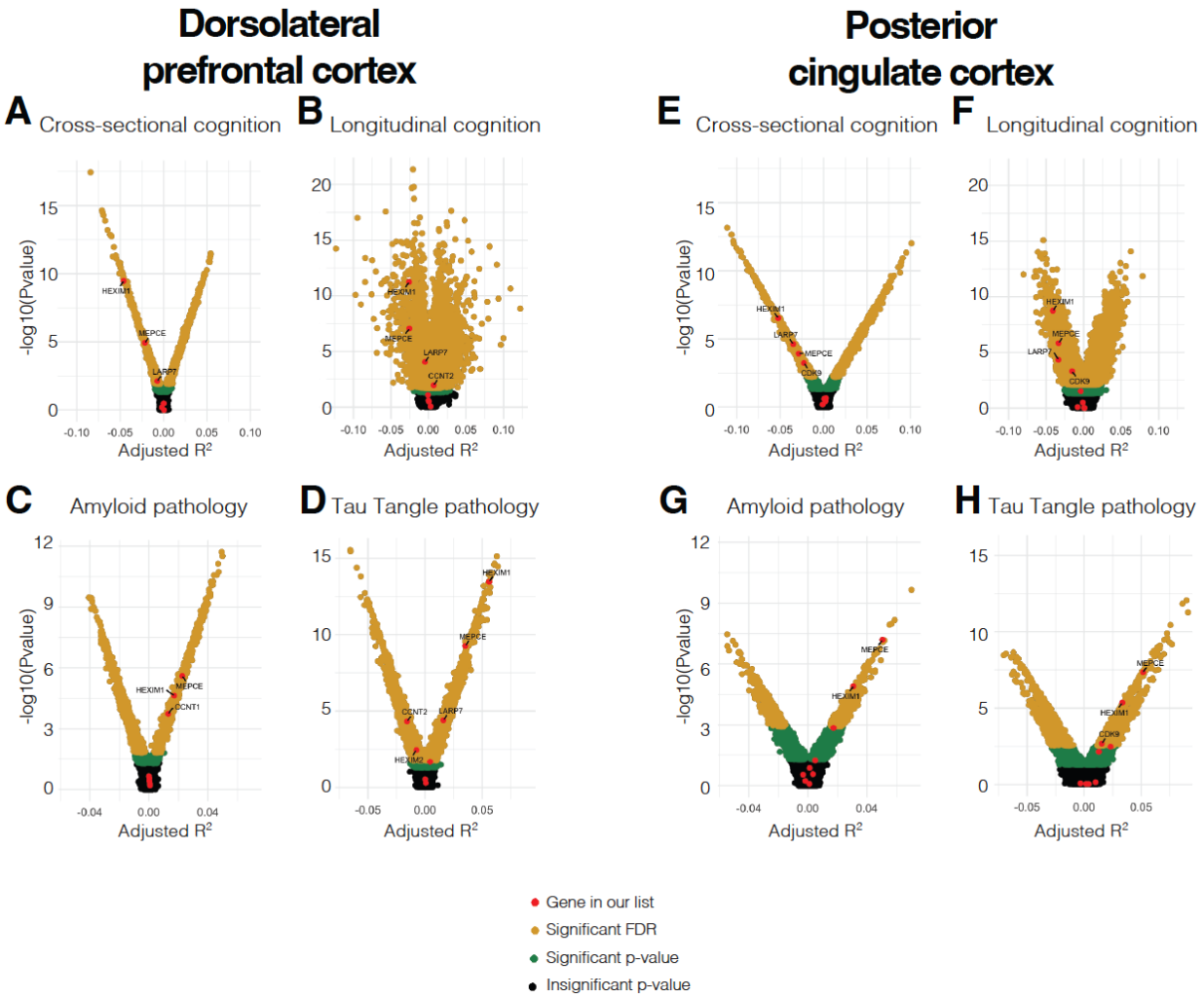

Supplementary Fig. 1. Correlations between P-TEFb regulatory complex components and AD-related phenotypes. Correlations of *BRD4*, *CCNT1*, *CCNT2*, *CDK9*, *HEXIM1*, *LARP7*, and *MEPCE* mRNAs with **A)** cross-sectional cognition, **B)** longitudinal cognition, **C)** amyloid pathology, and **D)** Tau tangle pathology in dorsolateral prefrontal cortex. Correlations of *BRD4*, *CCNT1*, *CCNT2*, *CDK9*, *HEXIM1*, *LARP7*, and *MEPCE* mRNAs and *RN7SK* non-coding RNA with **E)** cross-sectional cognition, **F)** longitudinal cognition, **G)** amyloid pathology, and **H)** tau tangle pathology in posterior cingulate cortex. Individual dots represent a single gene, and genes in the yellow region of the volcano plots are significantly correlated with the indicated pathology (FDR < 0.05).

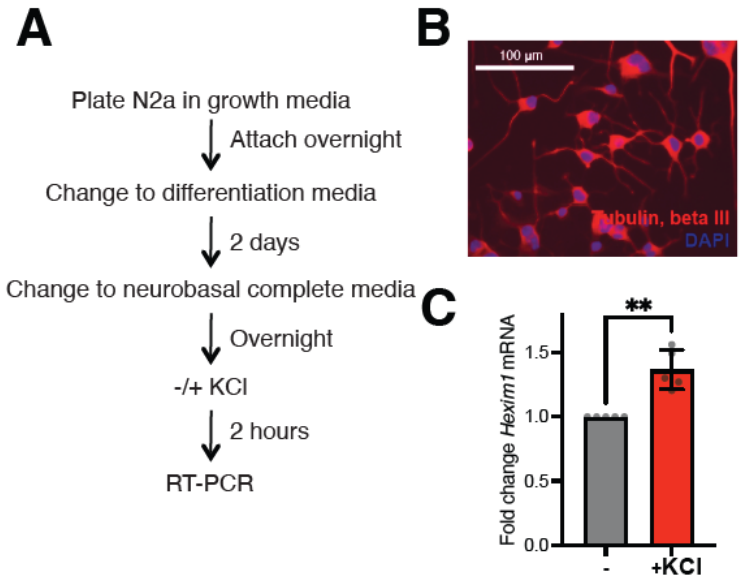

Supplementary Fig. 2. N2a cell differentiation procedure and KCl stimulation. A) Timeline of N2a plating, differentiation, and stimulation. **B)** ICC of a neuronal marker (TUJ1) in dN2a.**C)** RT-PCR of *Hexim1* mRNA after KCl stimulation in dN2a. n=6 biological replicates. One sample t test. $^{**}p<0.01$. Error bars represent standard deviation.

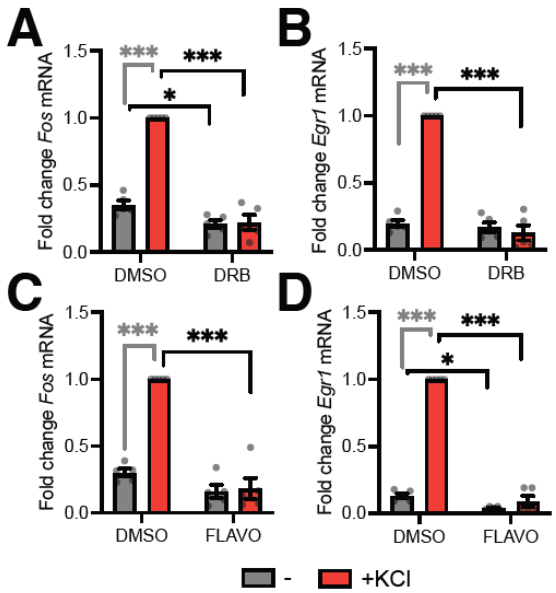

Supplementary Fig. 4. P-TEFb regulates activity-dependent IEG induction in dN2a. A) *Fos* and **B)** *Egr1* mRNA levels (RT-PCR) after pretreatment with DRB followed by KCl stimulation in dN2a. **C)** *Fos* and **D)** *Egr1* mRNA levels (RT-PCR) after pretreatment with FLAVO followed by KCl stimulation in dN2a. n=5 biological replicates. Two-way ANOVA with Sidak's multiple comparisons test. *p<0.05, ***p<0.001. Error bars represent standard deviation.

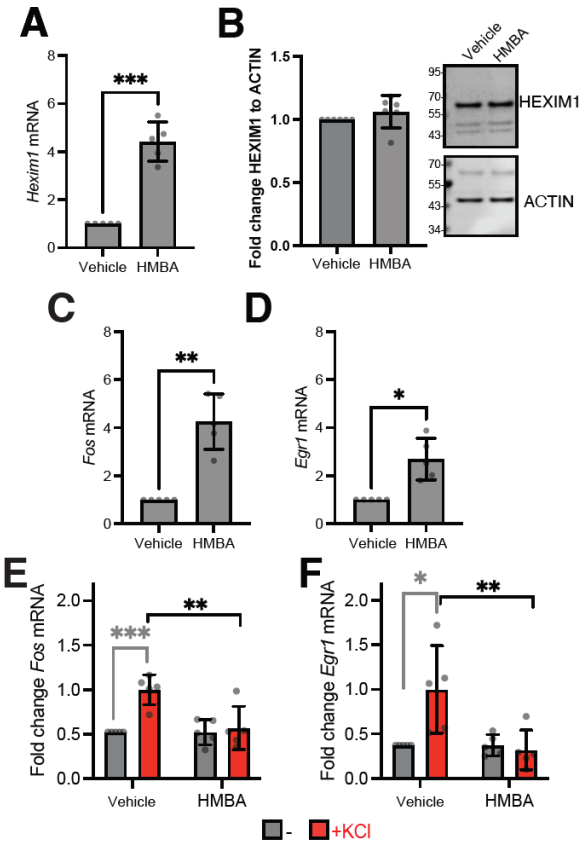

Supplementary Fig. 5. Effect of precluding HEXIM1/P-TEFb interaction with HMBA on baseline and inducible gene expression in dN2a. A) *Hexim1* mRNA expression changes after HMBA treatment (RT-PCR). n=5 biological replicates. **B)** HEXIM1 protein changes after HMBA treatment (Western blot). n=6 biological replicates. Representative blot to the right. **C)** *Fos* and **D)** *Egr1* mRNA expression changes in dN2a after HMBA treatment (RT-PCR). n= 5 biological replicates. One sample t test *p<0.05, **p<0.01, ***p<0.001. **E)** *Fos* and **F)** *Egr1* mRNA expression changes after HMBA followed by KCl stimulation in primary neurons. HMBA conditions were renormalized by dividing by the fold increase that HMBA caused alone to account for the baseline changes induced by HMBA. n=5 biological replicates. Two-way ANOVA with Sidak's multiple comparisons test. **p<0.01, ***p<0.001. Error bars represent standard deviation.

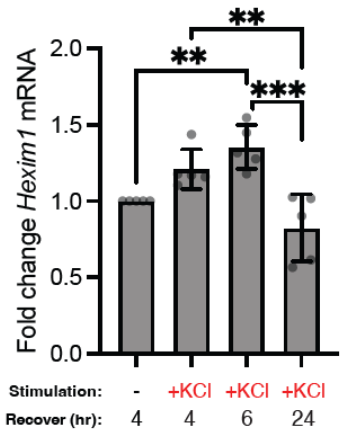

Supplementary Fig. 6. *Hexim1* mRNA during recovery from stimulation in dN2a. RT-PCR of *Hexim1* relative to *Hprt* mRNA following 2 hr. KCl stimulation and recovery for the indicated number of hours. n=5 biological replicates. One-way ANOVA with Tukey's multiple comparisons test. n=5 biological replicates. *$p<0.05$, **$p<0.01$. Error bars represent standard deviation.

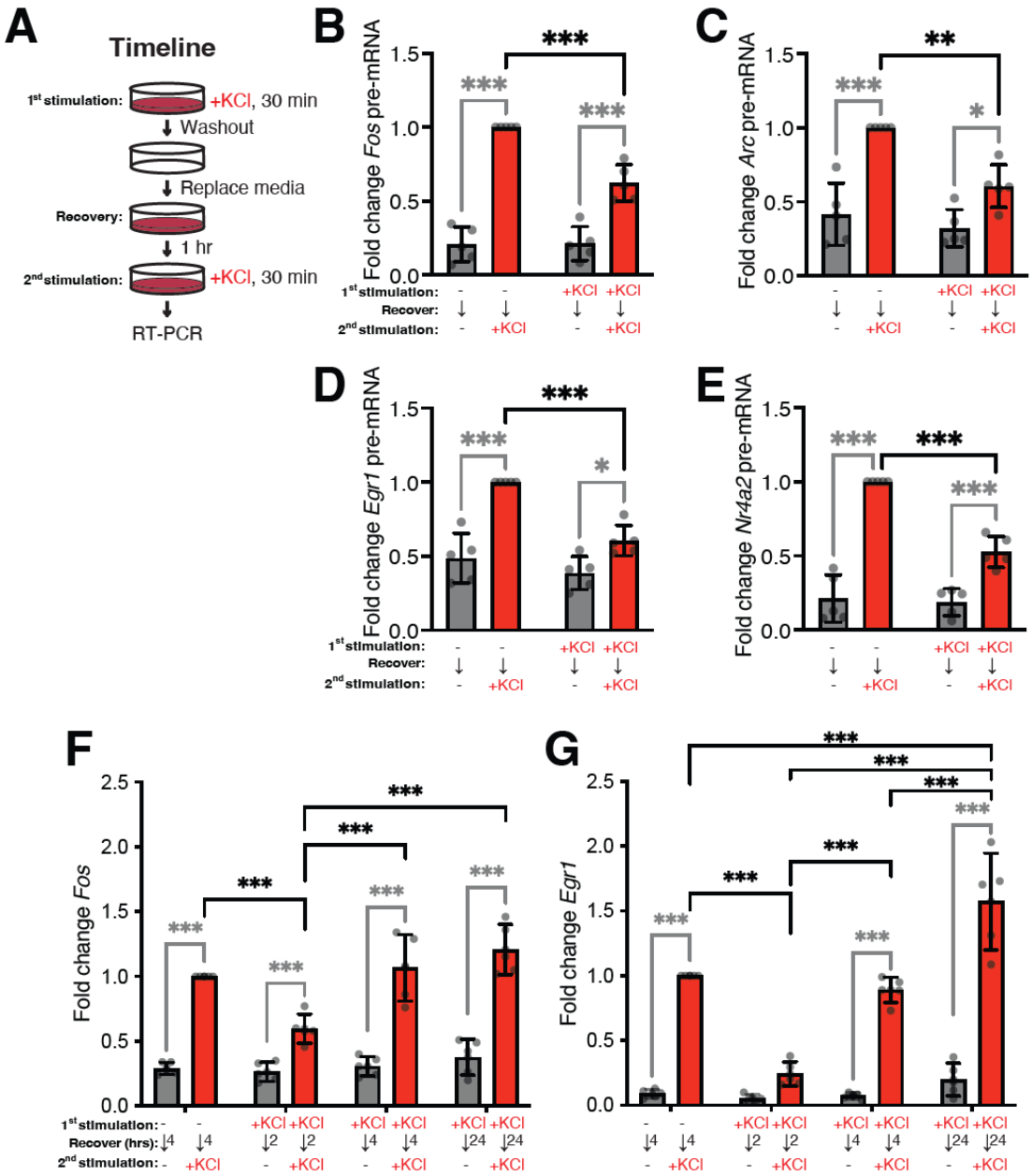

Supplementary Fig. 7. Transcriptional responses of IEGs are dampened following a prior stimulation in primary neurons and in dN2a. A) Timeline of 25mM KCl stimulations in **B-E**. **B)** *Fos*, **C)** *Arc*, **D)** *Egr1*, **E)** *Nr4a2* pre-mRNA expression (RT-PCR) in primary neurons during restimulation. IEG responses of **F)** *Fos* and **G)** *Egr1* mRNA in dN2a treated with 50mM KCl according to timeline described in **Fig. 7A** (RT-PCR). n=5 biological replicates. Two-way ANOVA with Sidak's multiple comparisons test. *p<0.05, **p<0.01, ***p<0.001. Error bars represent standard deviation.

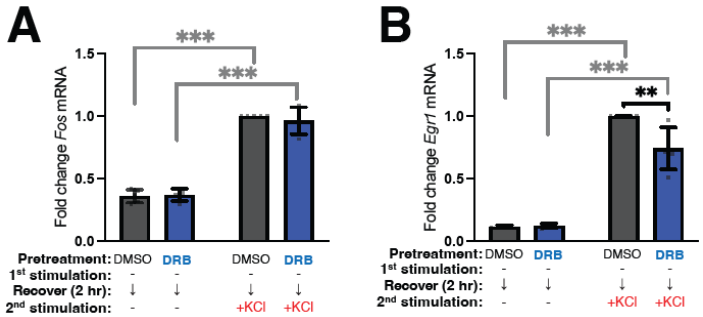

Supplementary Fig. 8. Effect of DRB pretreatment and washout on *Fos* and *Egr1* inducibility. Following the timeline depicted in **Fig. 8A**, we also measured the effect of vehicle (DMSO) or DRB pretreatment on **A)** *Fos* and **B)** *Egr1* mRNA expression levels (RT-PCR) in unstimulated (left two bars) or stimulated (right two bars) dN2a. Calculated as a fold change relative to KCl treatment during the second stimulation with no prior drug or KCl treatments. Two-way ANOVA with Tukey's multiple comparisons test. $^{**}p<0.01$, $^{***}p<0.001$. n=5 biological replicates. Error bars represent standard deviation.